Original research article

Evaluation of electronic transport and optical response of two-dimensional Fe-doped TiO2 thin films for photodetector applications

Fatih Kara[a], Mustafa Kurban[b,*], Burhan Coşkun[a]

[a] Department of Physics, Faculty of Science, Kırklareli University, Kırklareli, Turkey
[b] Department of Electronics and Automation, Kırşehir Ahi Evran University, Kırşehir, Turkey

ARTICLE INFO

ABSTRACT

We have carried out the structural, electronic and optical properties of Iron (Fe)-doped TiO2 thin films by sol-gel technique. The results reveal that the thin films form in a granular structure where particle-like grains cover the surface. Photophysical features of the thin films are performed by UV–vis spectrometry. The optical bandgap of undoped TiO2 thin film decreases from 3.17 eV to 3.05 eV with an increase in atomic ratios of Fe content, so the electron transfer is easier from the valence band to the conduction band. The current-voltage (I–V) and capacitance-voltage (C–V) characteristics of the undoped and Fe-doped TiO2 thin films are investigated under dark and various lighting intensities. Our results show that the photocurrents increase with increasing intensities of illumination. The photodiodes also show a decreasing capacitance with increasing frequency. From I–V and C–V plots, the photodiodes show rectifying properties and good photovoltaic behavior. Herein, the results display that the produced new Fe-doped TiO2 thin film samples can be used for photodetector applications.

1. Introduction

Nanostructures are finding use in many areas including energy, electronics, catalysis and sensors [1,2] due to their unique shape dependence properties when compared to their bulk structure [3]. More specifically, semiconductor metal-oxides exhibit important properties useful for a wide range of practical applications. Titanium dioxide (TiO2), in particular, has been investigated in recent years because it has excellent photophysical properties such as low cost, non-toxicity, high refractive index and chemical stability.

In these regards, TiO2 has been focused on many applications such as gas sensors due to its tunable electrical conductivity and photocatalytic properties [4,5]. TiO2 as a two-dimensional material at nanolevel has also been prepared by different experimental methods such as sol-gel [6–10] and reactive sputtering methods [11]. Recently, a fabrication of TiO2 nanoparticles (NPs) has been reported by an effective and inexpensive technique [12] to use them in photovoltaic devices.

Studies in the literature have shown that substitution of an atom on materials provides desirable physical and optical properties rather than their pure forms [13–15]. In this context, many efforts have been carried out on (X = Se, Cu, N, Fe, etc.)-doped TiO2 materials at the nanolevel [16–19] to perform the effects of the substitution an atom on the structural, electrical and optical features of pure TiO2. Thus, in this study, pure, 1 %, 5 % and 10 % Fe-doped TiO2 sol-gel mixtures were prepared; mixture then coated on a p-type silicon substrate using spin coating technique. Al contact was prepared using DC magnetron sputtering to obtain the final form of

---

* Corresponding author.
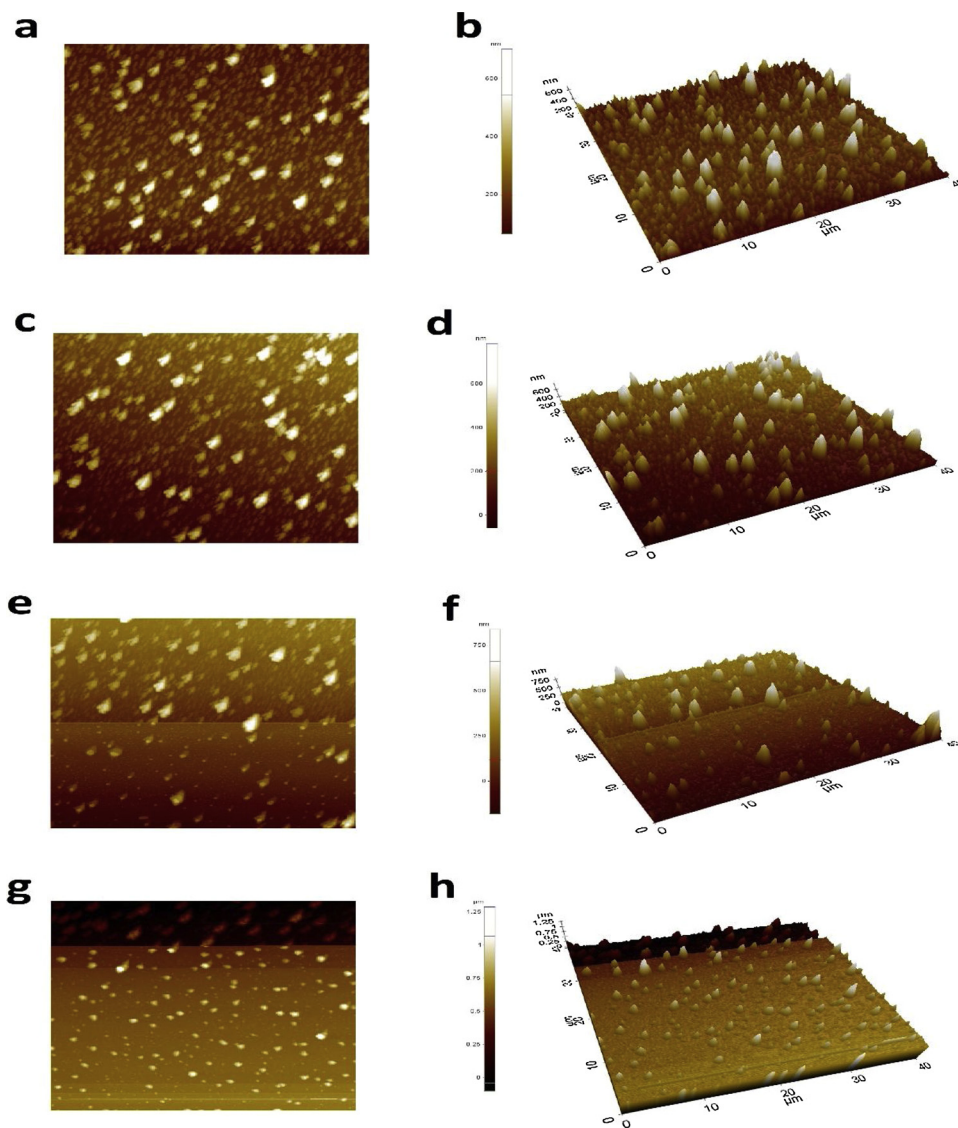E-mail addresses: mkurban@ahievran.edu.tr, mkurbanphys@gmail.com (M. Kurban).

Fig. 1. AFM images of undoped TiO_2 in 2D (a) and 3D (b), 1%Fe doped TiO_2 in 2D(c) and 3D(d), 5% Fe doped TiO_2 in 2D(e) and 3D(f), 10 %Fe doped TiO_2 in 2D(g) and 3D(h) were presented.
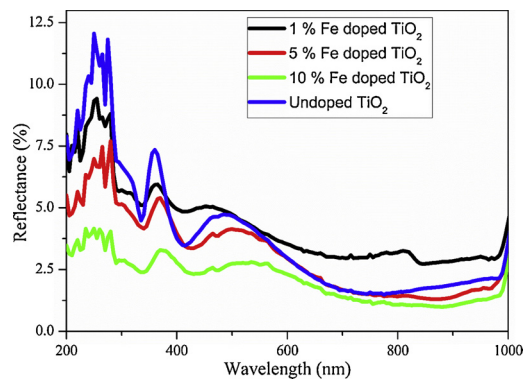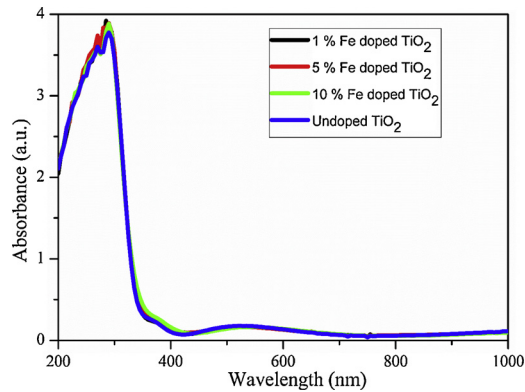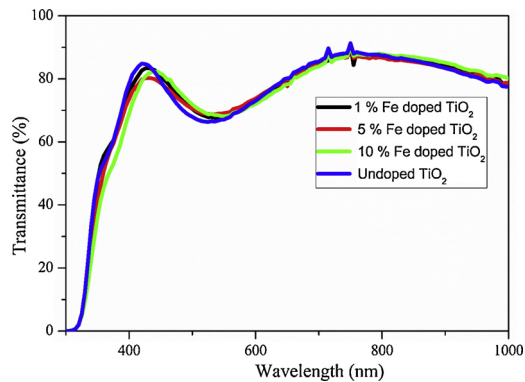

Fig. 2. The Reflectance spectra of undoped and Fe-doped TiO_2 samples.

Table 1

The average grain heights and maximum heights of undoped and Fe-doped TiO_2 thin films.

	Undoped TiO_2	1%Fe Doped TiO_2	5%Fe Doped TiO_2	10 %Fe Doped TiO_2
Average Grain Height (nm)	150	200	220	600
Maximum Height (nm)	558	609	558	977

Fig. 3. The absorption spectra of undoped and Fe-doped TiO_2 samples.

Fig. 4. The transmittance spectra of undoped and Fe-doped TiO_2 samples.

photodetectors to get TiO_2 thin films. Analysis of surface properties of the TiO_2 films was analyzed using the atomic force microscopy (AFM). Therefore, the goal of the research was to assess the dopant effect on surface, electric and optic properties of photodetectors. Photophysical features of the thin films were assessed with UV–vis spectrophotometric method; electrical and photovoltaic properties were investigated using FYTRONIX solar simulator.

2. Experimental

Fe doped TiO_2 solutions were produced by the sol-gel method and p-type Si substrates were coated using a spin coating method. In the preparation of the TiO_2 sol-gel mixture, four different 0,5 M Titanium Isopropoxide acetate solutions were dissolved in 10 mL ethanol (EtOH). Iron (III) nitrate with mole ratios of 1 %, 5 % and 10 % was added to three different TiO_2 solutions and mixtures were stirred by magnetic stirrer at 500 rpm. When dopants dissolved in solution, 0,5 mL HCl was added to the solutions as a stabilizer. Final solutions were stirred for 1 h at room temperature. To clean p-type silicon wafers from residual contamination, a chemical cleaning protocol was performed. Si substrates were first sonicated in alcohol five minutes and then, transferred to the water and sonicated five more minutes. After the sonication process, Si wafers dried with nitrogen gas. Clean Si wafers were transferred to spin coater, TiO_2, 1% Fe doped TiO_2, 5 % Fe doped TiO_2, 10 % Fe doped TiO_2 mixtures were dropped cast on different wafers. Mixtures were spin-coated twice at 3500 rpm for 30 s. To evaporate residual ethanol on the mixture, thin films were dried at 120 °C for 5 min. Final products were annealed at 450 °C for 1 h. Al contacts were prepared by PVD-HANDY/2S-TE (Vaksis Company) vacuum thermal evaporation in the pressure of 4.5×10^{-5} Torr where Al/TiO_2/p-Si/Al and Al/Fe:TiO2/p-Si/Al photodiodes were obtained. The surface properties of the thin films were investigated using PARK SYSTEM XE-100E atomic force microscope (AFM) in non-contact mode at room temperature in ambient conditions. The optical properties of the thin films were assessed at room temperature using
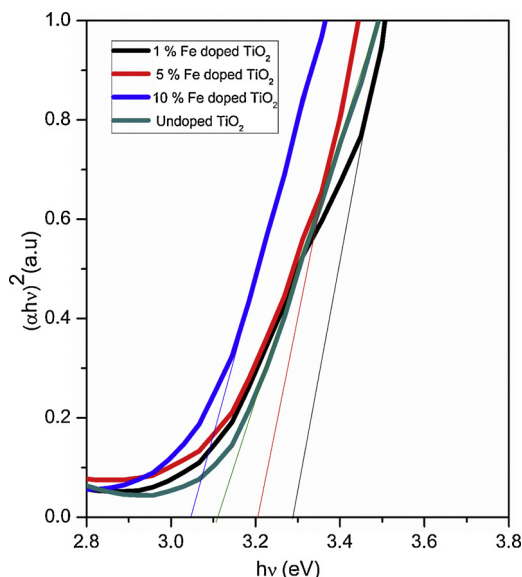
Fig. 5. The $(\alpha h\nu)^2 - h\nu$ graphs of undoped and Fe-doped TiO$_2$ samples.

SHIMADZU UV–vis–NIR 3600 spectrophotometer in the wavelength between 200 and 1000 nm. Electric and optoelectronic properties of photodiodes were investigated using FYTRONIX FY-7000 Solar Simulator I–V Characterization System.

3. Results and discussions

3.1. Surface characterization

AFM images which are in the sizes 40 μm × 40 μm taken from the thin films were obtained in non-contact mode at room temperature in ambient conditions. Fig. 1 shows the surface topography of the structural properties of the samples measured with AFM. Initial investigations revealed that thin films form in a granular structure where particle-like grains covers the surface. Individual big clusters could be seen that they spread on the thin-film surface homogeneously. For the undoped TiO$_2$ films; height distribution shows the average particle height as 150 nm where maximum height was 558 nm. For the 1% Fe doped TiO$_2$ films, average height was found about 200 nm from the height distribution measurement; maximum cluster height was measured as 609 nm. For the 5 % Fe doped TiO$_2$ films, average particle height was obtained as 220 nm from the height distribution analysis where maximum cluster height was measured as 568 nm. For the 10 %Fe doped TiO$_2$, average height was obtained about 600 nm from the height distribution analysis; maximum cluster height was measured as 977 nm. The increased average height was obtained with an increased Fe doping rate.

3.2. Optical characterization

Optical properties of materials, such as reflectance, absorbance and transmittance, can be measured by the interactions between photon and material. Through our work, the optical analysis of the thin films was performed at $200 - 1000$ nm scanning zone and room temperature. Fig. 2 indicates the reflection spectra of the TiO$_2$ thin films. From Fig. 2, the reflection of the undoped TiO$_2$ thin films decreases with the increasing Fe doping rate. After 300 nm, the fluctuations decrease in terms of the increase in wavelength. Also, the reflection curves have a maximum peak at about 250 nm corresponds the near-visible region, which show a decreasing trend at the visible region with an increase in the content of Fe dopant and in the number of grain boundaries (see Table 1) giving rise to optical scattering because of decreasing of the sample size with Fe dopant. This means that the optical band gaps of the films vary in terms of Fe dopant. This phenomenon is related to an increase in the interactions among the atoms or molecules in the thin films.

Fig. 3 displays the absorption spectra of undoped and Fe-doped TiO$_2$ samples. It was observed that there is an increasing trend in absorbance values up to about 300 nm which represents absorbance maxima. After 300 nm, a sharp decrease occurred, and then a weak increase in the visible region. Our results show that the 1 % Fe-doped ZnO sample has the highest absorption value than the others. An increase in the content of Fe dopant gives also rise to an increase in absorption values. The band edge becomes shifted to a lower wavelength side (higher energy) with a dopant Fe atom because of the dependence of Fe dopant on the Burnstein-Moss effect [20].

The optical transmittance spectra of the films were displayed in Fig. 4. The effects of the Fe dopant on the absorption spectra were observed with a sharp increase in the absorption band between 300 and 500 nm. All of the undoped and doped-TiO$_2$ thin films indicate a transmittance of more than 80 % in the visible region. However, the optical transmittance values decreased up to below 70
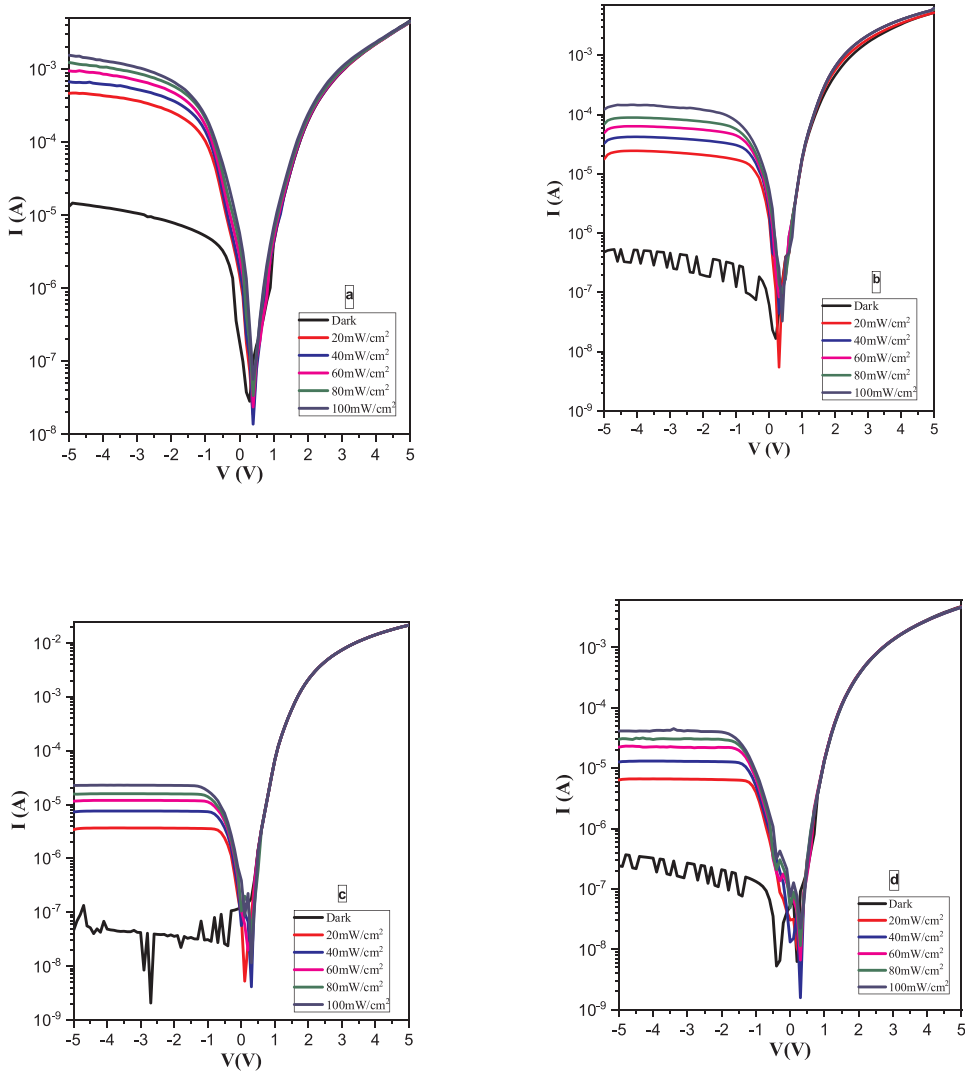
Fig. 6. The Current (I)-Voltage (V) characteristics in the samples a) undoped TiO2 b) 1% Fe doped TiO2 c) 5 % d) 10 % for different illumination intensities.

% between 400 and 600 nm, which is probably due to between the valence band and the conduction band [21]. The undoped and Fe-doped TiO_2 thin films do not show permeability since they absorbed at the wavelengths higher than 400 nm.

The bandgap of materials, in particular, organic semiconductors is primary features to get information about their band structure and optical features. The optical band gap (E_{og}) can be estimated from Tauc model given by [22]

$$\alpha(h\vartheta) = A(E - E_{og})^m \tag{1}$$

where α, $h\vartheta$ (and E), and A are the absorption coefficient, the photon energy and a constant, respectively and m determines the type of the optical transitions. The m is important to determine the type of transitions because the bandgap can be either direct or indirect. If the m is ½, it is called a direct band gap, if it is 1, it is called an indirect bandgap. In our study, we found m as ½ for quinoline derivatives, which corresponds to the allowed direct bandgap. We plotted the $(\alpha h\vartheta)^2$ curves in terms of energy (E) to examine bandgap morphology (see Fig. 5). Extrapolating the linear plot to $(\alpha h\vartheta)^2 = 0$, the E_{og} energies were measured as 3.17 eV, 3.28 eV, 3.08 eV, and 3.17 eV for the undoped and 1 %, 5 %, and 10 % Fe-doped TiO_2 thin films, respectively. From results obtained, the charge transfer mobility in the 10 % Fe-doped TiO_2 thin film is the smallest than that of the others. This means that it needs less excitation energy. When it comes to the values of energy gap, the TiO_2 thin films are close to the visible region.

3.3. The electrical characterization

The Current-Voltage (*I–V*) curves of the prepared thin films were carried out by different illumination intensities (see Fig. 6). Under forward-bias, the thin films indicate rectifying behavior, where the current increases dramatically in the 0.5–3 V region. Such a
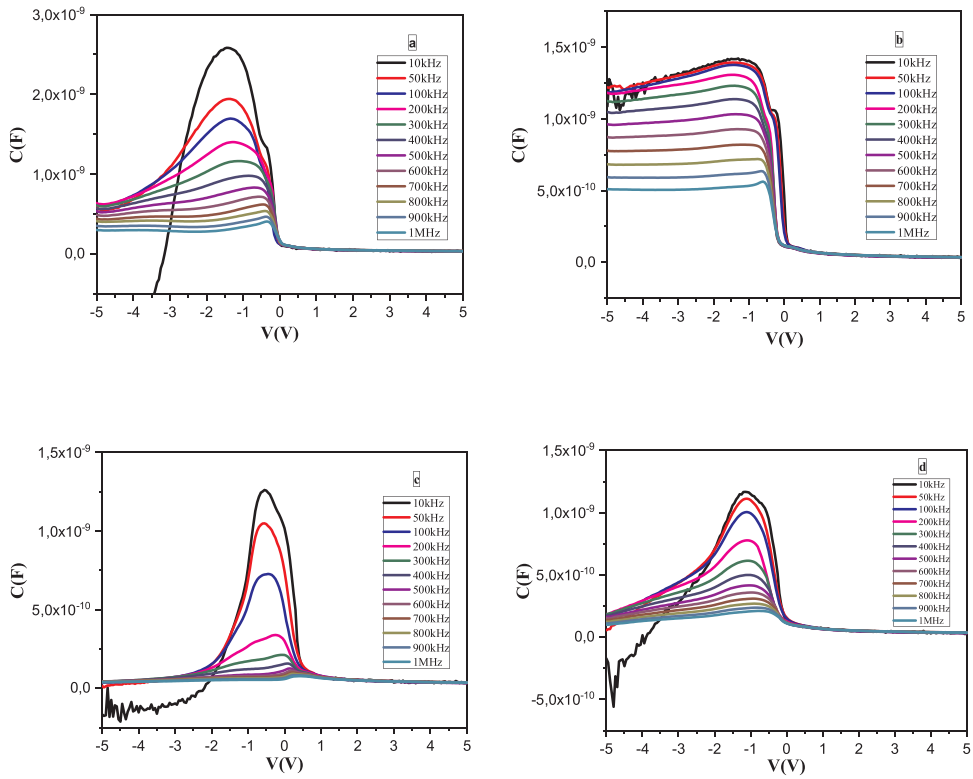
Fig. 7. The Capacitance (C)/Voltage (V) variation in the samples a) undoped TiO2 b) 1% Fe doped TiO2 c) 5 % d) 10 %.
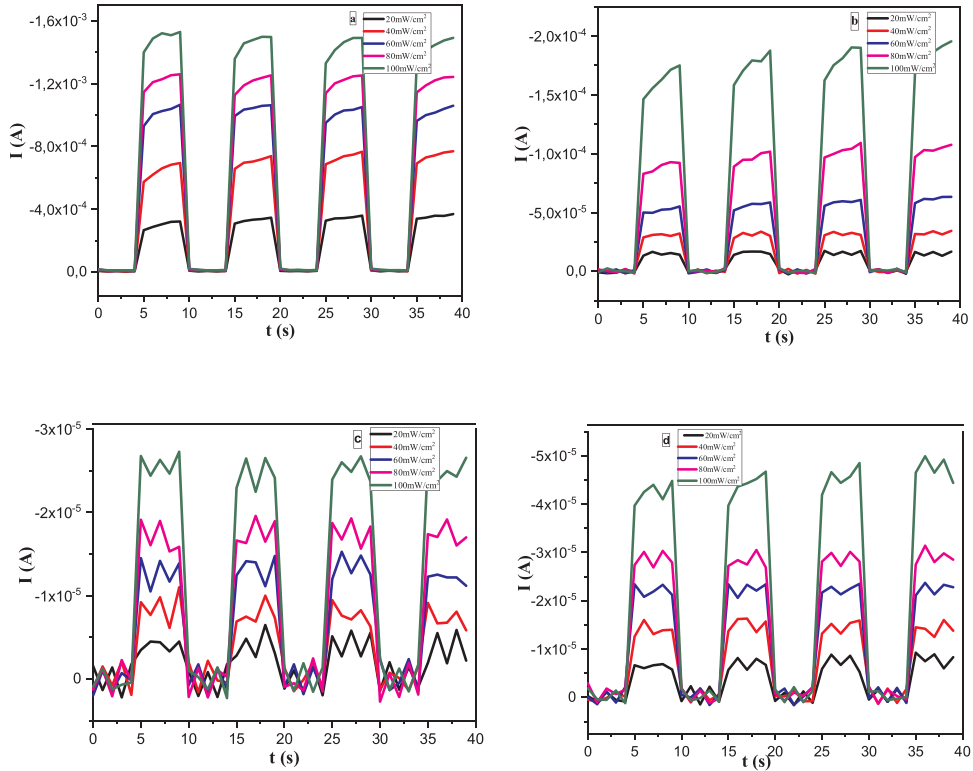

Fig. 8. The Current (I)/Time (t) variation in the samples a) undoped TiO2 b) 1 % Fe doped TiO2 c) %5 d) %10.

current difference obtained for illumination indicates that diodes show photovoltaic properties. Frequency and voltage dependence on the capacitance (C–V) of the undoped and Fe-doped TiO_2 thin films was also searched (see Fig. 7) between the 10 kHz and 1 MHz range. In the reverse region, as the frequency of the voltage applied to the capacitor increases, its effect is to decrease its capacitance. Thus, strong separation at measured capacitance was observed for 10 kHz, 50 kHz and 100 kHz. Decreasing the frequency, the separation between C–V plots seems larger than that of higher ones. Based on the increase in the frequency, the separation decreased and the change in capacitance for different frequencies indicates that the thin films were sensitive to AC signal at low frequencies, especially an increase in the content of Fe dopant. The frequency sensitivity plot of the diode also shows that the reverse-bias region was mainly induced by the minority carriers (holes, in this case) in the undoped and Fe-doped thin films. Furthermore, the bias region capacitance drops dramatically, and the separation between C–V plots for different voltage signal frequencies was diminished. Overall, the C–V characteristics obtained for the thin films show typical photodiode behavior. Also, C–V characteristics of 5 % Fe-doped TiO_2 are considerably different than that of the others because they slightly increase up to −1 V, then a sharp decrease up to 0 V.

In Fig. 8, the transient photo response behavior of the TiO_2 thin films is shown. The photocurrent-time measurement was carried out at −4 V. Fig. 8 indicates that the current rapidly increases after illumination and it remains constant until the illumination is subsequently turned off. The peak height of the photocurrent for the Fe-doped TiO_2 thin films also increases with an increase in illumination intensities. In conditions of darkness, the minimum current of the photodetector is measured, whilst illumination intensities of 20, 40, 60, 80 and 100 mW/cm^2 give rise to an increase in photodiode currents. When it comes to an increase in Fe dopant, the current and fluctuations gradually increase.

4. Conclusion

We investigated the structural, morphological and optical features of the undoped and Fe-doped TiO_2 thin films produced with the sol-gel method. Surface characteristics of the photodiodes were characterized using AFM. Optoelectronic features of the photodiodes were assessed. Using UV–vis spectra, bandgap energies of the diodes were carried out and the effect of Fe doping on TiO_2 thin films bandgap energies was assessed. It was seen that Fe doping decreases the bandgap energies. I−V characteristics illustrate that diodes show rectifying characteristics. I – t characteristics of photodiodes indicate that diodes show good photovoltaic characteristics where increased photocurrent was obtained for increased illumination intensities. Decreased capacitance for increased AC signal frequency was observed in the C−V assessment of the photodiodes. Prominent peaks were observed for certain frequency degrees at certain voltage ranges (between 0 V and −1 V), especially for Fe doped TiO_2 diodes.

Acknowledgments

References

[1] D. Chakravorthy, A.K. Giri, C.N.R. Rao (Ed.), Chemistry of Advanced Materials, Blackwell, Oxford, 1993, p. 217.
[2] U. Schuberf, S. Tewinkel, R. Lamber, Chem. Mater. 8 (1996) 2047.
[3] K. Karthik, S. Kesava Pandian, N. Victor Jaya, Appl. Surf. Sci. 256 (2010) 6829e6833.
[4] H.A. Macleod, Thin Optical Filters, second ed., MacMillan, New York, 1986.
[5] G. Sberveglieri (Ed.), Gas Sensors, Klewer Academic Publishing House, Dordrecht, 1992.
[6] A.K. Hassan, N.B. Chaure, A.K. Ray, A.V. Nabok, S. Habesch, J. Phys. D Appl. Phys. 36 (2003) 1120.
[7] J. Yu, X. Zhao, J. Du, W. Chen, J. Sol Gel Sci. Tech. 17 (2000) 163.
[8] B. Liu, X. Zhao, Q. Zhao, C. Li, X. He, Mater. Chem. Phys. 90 (2005) 207.
[9] Ü.A. Arıer, F.Z. Tepehan, Surf. Coat. Technol. 206 (2011) 37 Ö.
[10] J. Medina-Valtierra, M.S. Cardenas, C.F. Reyes, S. Calixto, J. Mex, Chem. Soc. 50 (2006) 8.
[11] M. Stamate, G.I. Rusu, I. Vascan, SPIE, vol. 3405-0277-786X/98/951e954.
[12] M. Ramazani, M. Farahmandjou, T.P. Firoozabadi, Phys. Chem. Res. 3 (2015) 293.
[13] İ. Muz, M. Kurban, Opto-Electronics Rev. 27 (2019) 113–118.
[14] İ. Muz, M. Kurban, J. Alloys. Compd. 802 (2019) 25–35.
[15] M. Kurban, Optik 172 (2018) 295–301.
[16] Wei Xie, Rui Li, Qingyu Xu, Sci. Rep. 8 (2018) 8752.
[17] Nazli Turkten, Zekiye Cinar, Ayse Tomruk, Miray Bekbolet, Environ Sci Pollut Res (2019), https://doi.org/10.1007/s11356-019-04474-x.
[18] Xiuwen Cheng, Xiujuan Yu, Zipeng Xing, Lisha Yang, Arab. J. Chem. 9 (2016) S1706–S1711.
[19] M.B. Marami, M. Farahmandjou, B. Khoshnevisan, J. of Elec Materi 47 (2018) 3741, https://doi.org/10.1007/s11664-018-6234-5.
[20] P.S. Kolhe, A.B. Shinde, S.G. Kulkarni, N. Maiti, P.M. Koinkar, K.M. Sonawane, J. Alloys. Compd. 748 (2018) 6–11.
[21] H. Aydin, C. Aydin, A.A. Al-Ghamdi, W.A. Farooq, F. Yakuphanoglu, Optik 127 (2016) 1879–1883.
[22] K. Cheng, J. Liu, R. Jin, J. Liu, X. Liu, Z. Lu, Y. Liu, X. Liu, Z. Du, Appl. Surf. Sci. 409 (2017) 124–131.